Experimental Design of Stand-alone Field Oriented Control for WECS in Variable Speed DFIG-based on Hysteresis Current Controller

Fayssal AMRANE[*,1,2], Azeddine CHAIBA[1], Bruno FRANCOIS[2] and Badreddine BABES[1]
[*, 1] LAS Research Laboratory Department of Electrical Engineering, University of Setif 1, Setif, Algeria.
[2] Laboratoire d'Electrotechnique et d'Electronique de Puissance de Lille (L2EP), Ecole Centrale de Lille, Lille, France.
E-mail : amrane_fayssal@live.fr.

***Abstract*— This paper presents the experimental design of a stand-alone field-oriented control (FOC) for wind turbine based on a doubly fed induction generator (DFIG). The control law is synthesized using a hybrid FOC-Hysteresis current controller (HCC) in Rotor side converter (RSC) and the stator is connected to the resistive load via rectifier (nonlinear load). The regulation is achieved below the synchronous speed (Hypo-synchronous mode). The implementation is realized using dSPACE1104 single board control and acquisition interface. The obtained results of the proposed control present high performance in steady and transient states.**

***Keywords*— Doubly fed induction generetor (DFIG), Field oriented control (FOC), Hysteresis current controller (HCC), Rotor/Stator side converter (RSC/SSC), dSPACE1104.**

I. INTRODUCTION

Several of the wind turbines today are equipped with double fed induction machine (DFIM). However, most of these machines are connected directly to the electrical network to avoid the presence of a converter [1-2]. The major advantage of these facilities lies in the fact that the power rate of the inverters is around the 25-30% of the nominal generator power [3-4]. A double fed induction generator (DFIG) consists of a wound rotor induction generator (WRIG) with the stator windings directly connected to a three-phase power grid and with the rotor windings mounted to a bidirectional back-to-back IGBT frequency converter [5]. Control strategies of DFIG have been discussed in details in literatures [6-7-8]. Control of DFIG through the Field Oriented Control (FOC) which is performed by rotor currents control has been developed in [9].

There are two famous methods for DFIGs employment in wind power systems such as: Stand-alone installation and Grid-connected usage. There are many papers, which have concentrated on doubly fed induction generators′ operation as grid-connected and stand-alone systems [10-11]. A comparative study on islanded and grid-connected operation of DFIG based wind generator has been presented in [11]. Most of the researchers in this area are concentrated on analyzing network dynamics, system transients, fault conditions, or grid disturbances' [12-13-14]. A schematic diagram of variable speed wind turbine system with a DFIG is shown in fig. 1. Vector control utilizes the dynamic state relationships of DFIG to define angu-

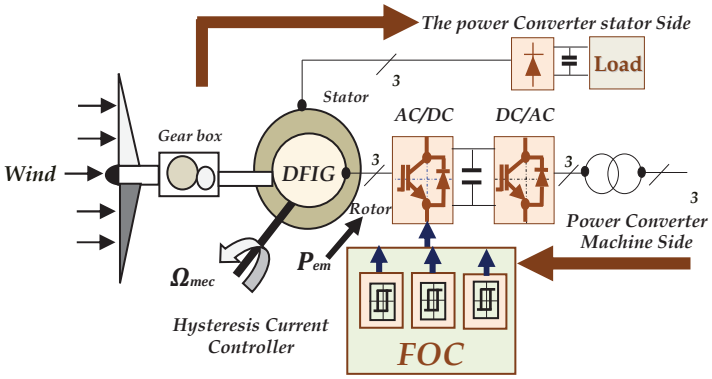

Fig.1 Schematic diagram of wind turbine system with a DFIG.

-lar speed, amplitude and instantaneous position of current, voltage and flux linkage vectors [11-12]. In contrast scalar control method proposition employs steady-state relationships to determine angular speed and amplitude of current, voltage and flux vectors [13-14]. In [15], the authors propose enhanced hysteresis-based current regulators in the field-oriented vector control of doubly fed induction generator (DFIG) wind turbines. This proposed hysteresis-based technique has excellent steady-state performances. In our work, we are interested by the stand-alone usage; we used the Hysteresis current controller (HCC) to obtain the switching command signals. The main contribution of this paper is the experimental validation of the proposed control FOC-HCC based on stand-alone to ensure good tracking of the predefined references regardless the wind speed changing.

This paper is organized as follows; mathematical model of DFIG is presented in section II. In section III, presents the field oriented control of DFIG which is based on the orientation of the rotor flux vector along the axis 'd'. Section IV presents topology of Hysteresis current controller. The diagram (case study) of the implementation is described in details in section V. In section VI, experimental results are shown and discussed. Finally, the reported work is concluded.

II. MATHEMATICAL MODEL OF DFIG

The generator chosen for the conversion of wind energy is a double-fed induction generator, DFIG modeling described in model of the induction machine obtained using Park the

two-phase reference (Park). The general electrical state transformation is given by the following equations, [16-17-18]:

Stator and rotor voltages:

$$V_{sd} = R_s * i_{sd} + \frac{d}{dt}\emptyset_{sd} - \omega_s * \emptyset_{sq} \quad (1)$$

$$V_{sq} = R_s * i_{sq} + \frac{d}{dt}\emptyset_{sq} + \omega_s * \emptyset_{sd} \quad (2)$$

$$V_{rd} = R_r * i_{rd} + \frac{d}{dt}\emptyset_{rd} - (\omega_s - \omega) * \emptyset_{rq} \quad (3)$$

$$V_{rq} = R_r * i_{rq} + \frac{d}{dt}\emptyset_{rq} + (\omega_s - \omega) * \emptyset_{rd} \quad (4)$$

Stator and rotor fluxes:

$$\emptyset_{sd} = L_s * I_{sd} + L_m * I_{rd} \quad (5)$$

$$\emptyset_{sq} = L_s * I_{sq} + L_m * I_{rd} \quad (6)$$

$$\emptyset_{rd} = L_r * I_{rd} + L_m * I_{sd} \quad (7)$$

$$\emptyset_{rd} = L_r * I_{rd} + L_m * I_{sd} \quad (8)$$

The electromagnetic torque is given by:

$$C_e = P * L_m * (I_{rd} * I_{sq} - I_{rq} * I_{sd}) \quad (9)$$

And its associated motion equation is:

$$C_e - C_r = J * \frac{d}{dt}\Omega + f * \Omega \quad (10)$$

$$J = \frac{J_{turbine}}{G^2} + J_g \quad (11)$$

where: C_r is the load torque J is total inertia in DFIG's rotor, Ω is mechanical speed and G is gain of gear box.

III. FIELD ORIENTED CONTROL (FOC)

In this section, the DFIG model can be described by the following state equations in the synchronous reference frame whose axis d is aligned with the rotor flux vector as shown in fig. 2, ($\emptyset_{rq} = 0$) and ($\emptyset_r = \emptyset_{rd}$)

$$I_{rq} = -\frac{L_m}{L_r} * I_{sq} \text{ and } I_{sq} = -\frac{L_r}{L_m} * I_{rq} \quad (12)$$

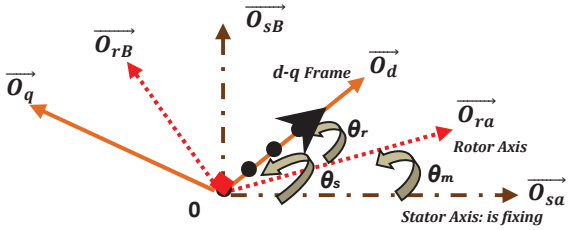

Fig. 2 Rotor flux vector in the synchronous d-q frame.

The rotor flux and the electromagnetic torque can be given by:

$$\emptyset_{sq} = -\sigma * \frac{L_s * L_r}{L_m} I_{rq} \quad (13)$$

$$C_{em} = P * L_m * (I_{sq} * I_{rd} - I_{sd} * I_{rq}) = -P * \emptyset_{rd} * I_{rq} \quad (14)$$

with: $\sigma = 1 - \frac{L_m^2}{L_s * L_r}$

$$If: \emptyset_{sq} = 0 \ (via\ stator) \Leftrightarrow \emptyset_{rd} = L_m * I_{sd} \quad (15)$$

$$If: I_{sd} = 0 \ (via\ rotor) \Leftrightarrow \emptyset_{rd} = L_r * I_{rd} \quad (16)$$

$$Via\ rotor\ and\ rotor \Leftrightarrow \emptyset_{rd} = L_r * I_{rd} + L_m * I_{sd} \quad (17)$$

where:

ϕ_{sd}, ϕ_{sq} are stator flux components, ϕ_{rd}, ϕ_{rq} are rotor flux components, V_{sd}, V_{sq} are stator voltage components, V_{rd}, V_{rq} are rotor voltage components. R_s, R_r are stator and rotor resistances, L_s, L_r are stator and rotor inductances, L_m is mutual inductance, σ is leakage factor, P is number of pole pairs, f is the friction coefficient.

The rotor side converter (*RSC*) representing by FOC and Hysteresis current topology is represented in details in fig.4. *Ird** is the image of flux, and *Irq** is the image of torque from the *MPPT (maximum power point tracking)*.

IV. HYTERESIS CURRENT CONTROLLER

T_i and T'_i are switches connected, one to the output of a hysteresis comparator, the other to this same output via an inverter. The sign of the difference of change between the reference and the measured current does not instantaneously results in the tilting of the comparison due to the effect of the hysteresis, which means the measured current is changing by increasing until ΔI is equal to h. The comparator switches over either switch comes into conduction in turn as $\Delta I < h$ illustrated in (fig.3.b). The switching conditions are defined in terms of logical states corresponding as below (fig.3.a) [10]:

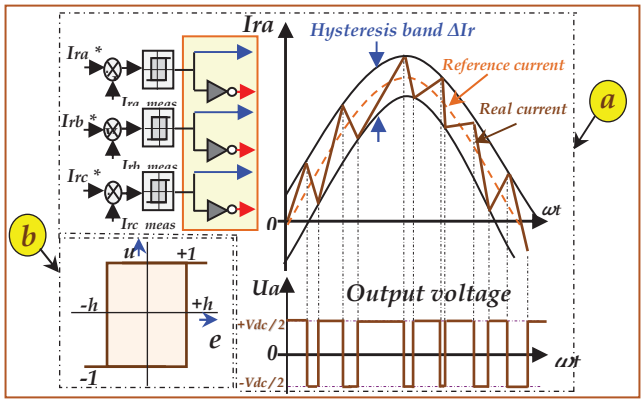

Fig. 3 Hysteresis current control topology.

$$S_i = -1 \quad if \quad I_i \geq I^* + \Delta I \quad (18)$$

$$S_i = +1 \quad if \quad I_i \leq I^* - \Delta I \quad (19)$$

$$S_i = S_{i-1} \quad if \quad I_i = I^* \quad (20)$$

with:

I_i $(i = 1, 2, 3)$, represent the currents of the stator phases.

I^* $(1, 2, 3)$, represent the reference currents from the control circuits of the inverter

V. CASE STUDY

Fig. 5 presents the experimental test bench developed in Automatic Laboratory of Setif (LAS), the DFIG (Doubly Fed Induction Generator) used in this real time implementation is a

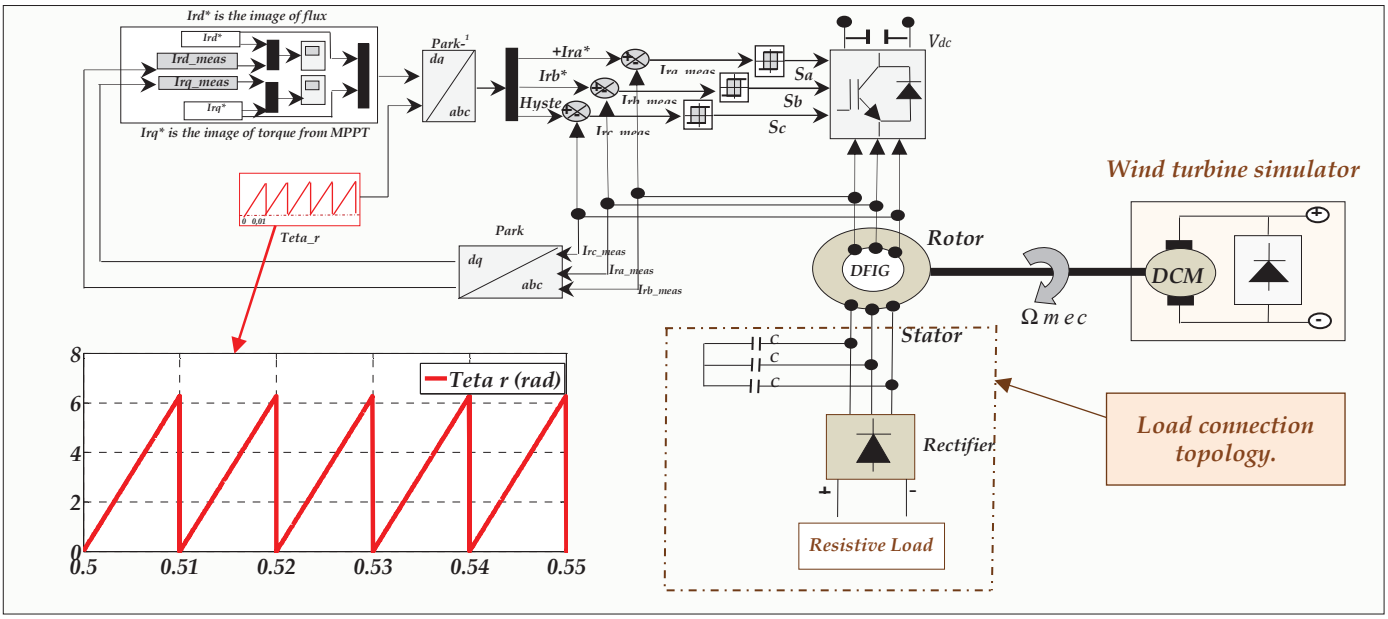

Fig. 4 Rotor side converter control system.

3.5 kW (whose parameters are indicated in table.1 and DCM (Direct Motor Current) is a 3kW.

Fig. 6 shows a diagram of test system. In the upper right is described the DFIG sub-system, composed of a 3.5kW, and in the upper left emulator turbine represented by 3kW DCM, as follows in fig.6.

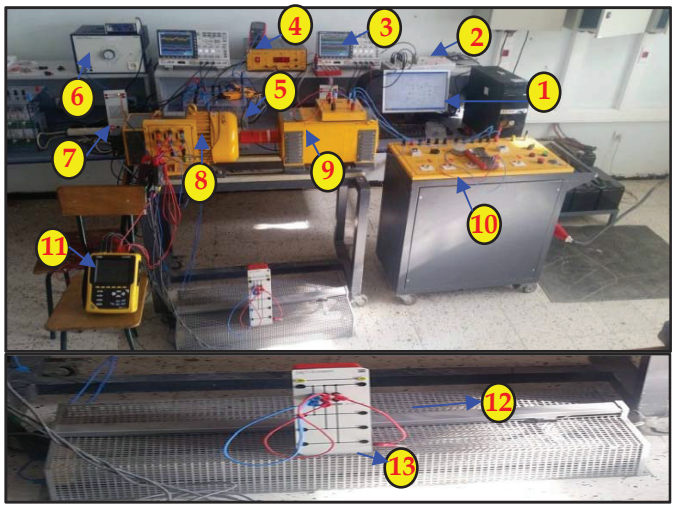

Fig. 5 Experimental test bench; 1: PC, 2: dSPACE 1104, 3: Oscilloscope, 4: Speed sensor, 5: Inverter (Semikron), 6: DC variable source, 7: DC 15 V source, 8: DFIG, 9: DCM, AC 380 V (Grid), 11: Power analyzer, 12: Resistive load, 13: Capacitor.

VI. Experimental Results And Discussion

The lower part of fig.6 is composed of a data acquisition system connected to the control board. The FOC algorithm is implemented on real time board (*dSPACERTI1104*) from Tex-

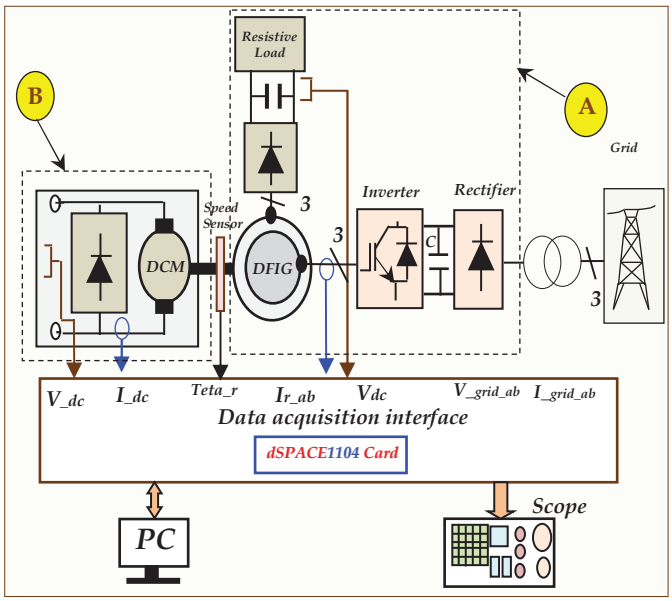

Fig. 6 Test system global topology.

as Instrument with a *TMS320F240 DSP* (*20 MHz*) and a microprocessor Power PC 603e (250 MHz); with a sampling time Ts= 50 µs (fixed step); the controller is executed at 20 k Hz.

The connections between the dSPACE card and the power converter are carried out by an interface card, which adapts the control signal levels. The current and voltage are ensured by the Fluke i30S and ST1000-II sensors respectively, whereas, both the rotor position and speed are given by a 1024-pulse incremental encoder implemented on the DC motor shaft (as shown in fig.5).

A. Rotor side converter (RSC) :

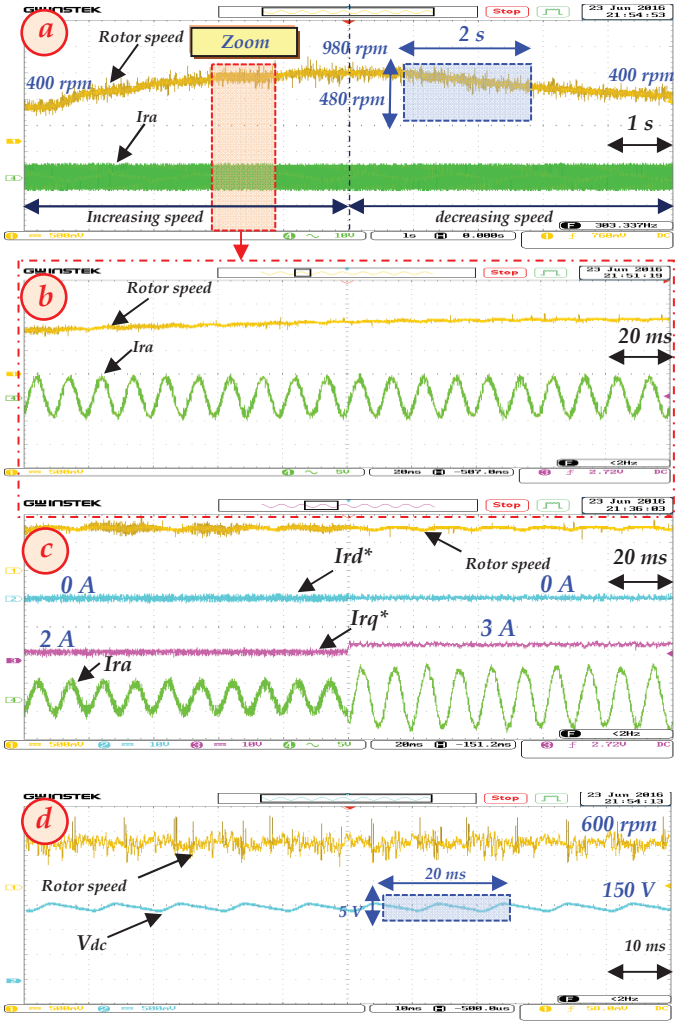

Fig. 7 (a) & (b): Steady and transient states respectively of increasing and decreasing rotor speed and rotor current, (c) variation of the rotor reference direct current, (d) transient and steady states of bus voltage.

B. *Grid side converter (GSC):*

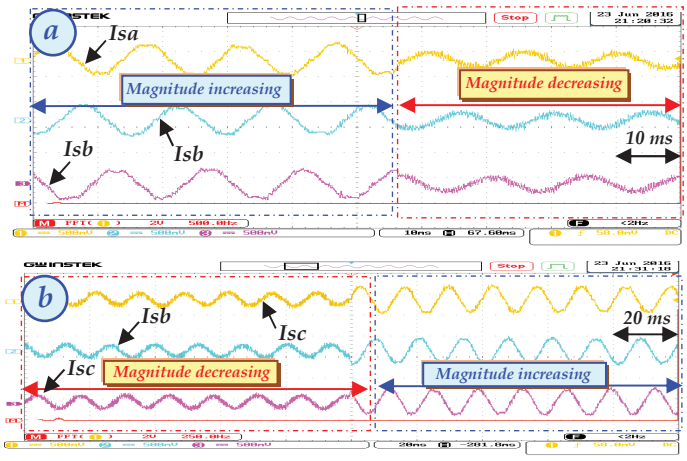

Fig. 8 (a): Stator currents Is, Isb, Isc under amplitude variation (the magnitude variation; increasing after decreasing), (b): Stator currents Is, Isb, Isc under amplitude variation (the magnitude variation; decreasing after increasing)

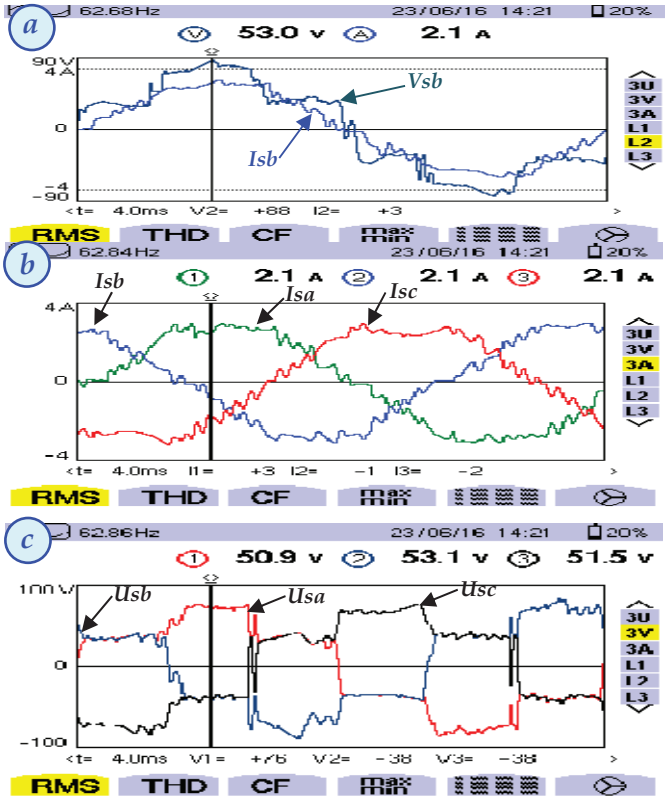

Fig. 9 Experimental measures obtained from power quality analyzer (a: Stator voltage Vsb (V) and stator current Isb (A), b: Stator currents Is_abc (A), c: compound stator voltages Us_abc (V).

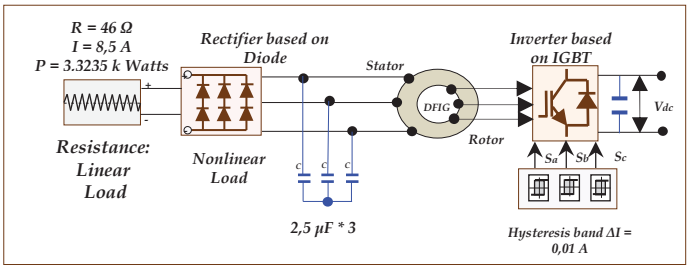

Fig. 10 Stand-alone DFIG topology.

In the rotor side converter (RSC), we used several tests, as shown in Fig.7. (a, b, c & d):

Fig.7.a shows the behavior of rotor speed (Ω_r (rpm)) and rotor currents (I_{rabc} (A)) under variation condition. The figure illustrates the variation (increasing) of speed from 400 (rpm) to 980 (rpm) (transient and steady state) during 5 (sec), less than synchronous speed (1420 (rpm)); and after that the decreasing of rotor speed from 980 (rpm) to 400 (rpm) during also 5 (sec), we remark the decreasing and increasing respectively of the rotor frequency currents. Fig.7.b presents the zoom of fig.7.a during 0.2 sec (=10 * 20 (msec)), it can be seen the sinusoidal form of the wave rotor current Ira (A). Fig.7.c illustrates the variation (increasing) of the reference transversal rotor current I_{rq}*(A) from 2 (A) to 3 (A); means the rotor torque with negative value to ensure the generator mode, on the other hand we keep the reference rotor direct current I_{rd}*(A) at zero value (0 (A)) means the image of the rotor flux

to ensure the exchange of the active power to the nonlinear load, in the same test the rotor speed is constant equals to 600 (rpm) during the variation of the currents references (I_{rd}*(A) and I_{rq}*(A)). Rotor current Ira (A) takes the sinusoidal form using the hysteresis current controller (with hysteresis band = +/- 0.01 (A)). The behavior of the bus voltage (V_{dc} = 150 (V)) and the rotor speed (Ω_r =600 (rpm)) are shown in fig.7.d during the stand-alone conditions.

In the Stator side converter (SSC), we used several tests, as shown in fig.8 (a & b) and fig.9. (a, b, & c):

Fig.8.a illustrates the behavior of the stator current under magnitude variation (decreasing amplitude) during the stand-alone topology, it can be seen the sinusoidal form of the three stator current (compound few ripple). Fig.8.b shows the variation of the stator currents under magnitude variation (increasing amplitude) during the stand-alone topology, it can be seen the sinusoidal form of the three stator currents (compound few ripple). Fig. 9 obtained from the power quality analyzer that shows the waves form of the stator currents and voltages under stand-alone conditions. Fig.9.a presents the behavior of stator current (Isb (A)) and the stator voltage (Vsb (V)) during stand-alone connection. Fig.9.b shows the sinusoidal stator currents Is_abc (A). Fig.9.c illustrates the stator compound voltage Us_abc (V) under stand-alone strategy. Fig. 10 presents the stand-alone DFIG topology, the stator is connected to the nonlinear load which compound by the unidirectional rectifier (based on six diodes) and resistive load ($R_{\_Load}$ = 46 (Ω) $I_{\_Load}$ = 8.5 (A), $P_{\_Load}$ = 3.325 (KWatts)) and the bank capacitance C=3* 2.5 (µF) used between the stator and the nonlinear load for voltage filtering.

APPENDIX

TABLE.1. PARAMETERS OF THE DFIG.

Rated Power:	*3.5 kWatts*
Stator Resistance:	*Rs = 2.3Ω*
Rotor Resistance:	*Rr = 6.95Ω*
Stator Inductance:	*Ls = 0.04 H.*
Rotor Inductance:	*Lr = 0.036 H.*
Mutual Inductance:	*Lm = 0.061 H.*
Rated Voltage:	*Vs = 220/380 V*
Number of Pole pairs:	*P= 2*
Rated Speed:	*N=1420 rpm*
Friction Coefficient:	f_{DFIG}*=0.00 N*m/sec*
The moment of inertia	*J=0.2 kg*m^2*

VII. CONCLUSION

In this paper, real time implementation of high performance field-oriented control for stand-alone of doubly fed induction generator is presented. The experimental test bench emulating a wind turbine and driving a DFIG allows validating experimentally the modeling and the control techniques. The performance of a hybrid Hysteresis-FOC is implemented in a real time via dSPACE 1104 card. The experimental obtained results validate the control strategy, and provide good tracking of the predefined references regardless the wind speed changing.

VIII. REFERENCES

[1] Fayssal Amrane, Azeddine Chaiba, "A Novel Direct Power Control for grid-connected Doubly Fed Induction Generator based on Hybrid Artificial Intelligent Control with Space Vector Modulation", *Rev. Roum. Sci. Techn.– Électrotechn. et Énerg*. Vol. 61, no.3, 2016.

[2] J. Mohammadi, S. Vaez-Zadeh, S. Afsharnia, E. Daryabeigi, "A Combined Vector and Direct Power Control for DFIG-based Wind Turbines", *IEEE Transactions on Sustainable Energy*, Vol. 5, no. 3, pp. 767–775, 2014.

[3] Heng Nian, Yipeng Song, "Direct Power Control of Doubly Fed Induction Generator under Distorted Grid Voltage", *IEEE Transactions on Power Electronics*, Vol. 29, no.2, 2014.

[4] Heng Nian, Peng Cheng, Z.Q. Zhu, "Coordinated Direct Power Control of DFIG System without Locked Loop under Unbalanced Grid Voltage Conditions", *IEEE Transactions on Power Electronics*, 2015.

[5] Roberto Cárdenas, Rubén Peña, Salvador Alepuz, Greg Asher, "Overview of Control Systems for the Operation of DFIGs in Wind Energy Applications", *IEEE Transactions on Industrial Electronics*, Vol. 60, no.7, 2013.

[6] J. Hu, J. Zhu, D. G. Dorrell, "Model-Predictive Direct Power Control of Doubly-Fed Induction Generators Under Unbalanced Grid Voltage Conditions in Wind Energy Applications, *IET Renewable Power Generation*, Vol. 8, no.6, pp. 687–695, 2014.

[7] Brice Beltran, Mohamed El Hachemi Benbouzid, Tarek Ahmed-Ali, "Second-Order Sliding Mode Control of a Doubly Fed Induction Generator Driven Wind Turbine", *IEEE Transactions on Energy Conversion*, Vol. 27, no.2, pp. 261-269, 2012.

[8] B. Bossoufi, M. Karim, A. Lagrioui, M. Taoussi, A. Derouich, "Observer Backstepping Control of DFIG-Generators for Wind Turbines Variable-Speed: FPGA-Based Implementation", *Renewable Energy*, Vol.81, pp.903–917, 2015.

[9] AG. Abo-Khalil, G. Ahmed, "Synchronization of DFIG output voltage to utility grid in wind power system", *Renewable Energy*, Vol.44, pp. 193-198, 2012.

[10] Fayssal Amrane, Azeddine. Chaiba, Badr Eddine Babes and Saad Mekhilef "Design and Implementation of high Performance Field Oriented Control for Grid-connected Doubly Fed Induction Generator via Hysteresis Rotor Current Controller", *Rev. Roum. Sci. Techn.– Électrotechn. et Énerg*. Vol. 61, no.4, pp.319-324, 2016.

[11] Zhou Y, Ferreira J A, Bauer P. "Grid-connected and islanded operation of a Hybrid power system", *IEEE Power Engineering Society Conference and Exposition in Africa*, Power Africa '07;2007.p.1–6.

[12] Morren J, de HaanS W H, "Ride through of wind turbines with doubly-fed induction generator during a voltage dip". *IEEE Transactions on Energy Conversion*, 2005.

[13] Kasem AH, El-Saadany EF, El Tamaly H H, Wahab M A A. "An improved fault ride-through strategy for doubly fed induction generator-based wind turbines". *IET Journal on Renewable Power Generation*, 2008.

[14] Buja GS, Kazmierkowski MP. "Direct torque control of PWM inverter-fed AC motors-asurvey". *IEEE Transactions on Industrial Electronics* 2004; 51:744–57.

[15] Quang N, Dittrich A, Thieme A. "Doubly-fed induction machine as generator: control algorithms with decoupling of torque and power factor".*Electrical Engineering (Archiv fur Elektrotechnik),* 1997.

[16] Fayssal Amrane, Azeddine Chaiba, "Type2 Fuzzy Logic Control: Design and Application in Wind Energy Conversion System based on DFIG via Active and Reactive Power Control", *Nova Science Publishers, Chapter-1*, pp.1-35, 2017.

[17] Fayssal Amrane, Azeddine Chaiba, Saad Mekhilef, "High performances of Grid-connected DFIG based on Direct Power Control with Fixed Switching Frequency via MPPT Strategy using MRAC and Neuro-Fuzzy Control", *Journal of Power Technologies*, Vol. 96, no. 1, pp.27-39, 2016.

[18] Mansour Mohseni, Syed M. Islam, Mohammad A. S. Masoum "Enhanced Hysteresis-Based Current Regulators in Vector Control of DFIG Wind Turbines". *IEEE Transactions on Power Electronics*, Vol. 26, pp. 223-234, 2011.